

Simulation Investigations of High Power Overmoded Relativistic Backward Wave Oscillator with Trapezoidal Resonant Reflector

V. Venkata Reddy, M.A. Ansari, and M. Thottappan*

Department of Electronics Engineering, Indian Institute of Technology (BHU), Varanasi - 221 005, India

*E-mail: mthottappan.ece@iitbhu.ac.in

ABSTRACT

An S-band high power relativistic backward wave oscillator using a trapezoidal resonant reflector and overmoded slow-wave structure is demonstrated by finite difference time domain based Particle-In-Cell code. The trapezoidal resonant reflector and slow-wave structure are chosen to improve the RBWO power handling capability to gigawatt (GW). The Trapezoidal resonant reflector enhances the pre-modulation during electron beam propagation, thus increasing the generated RF signal overall efficiency and coherency. The particle-in-cell simulation generated an RF output power ~ 5.4 GW in TM_{01} mode at ~ 3.6 GHz in a 2.0 T magnetic field and developed a 13.5 kA current for a 1.2 MV DC cathode voltage. The power conversion efficiency is achieved as ~ 33 %. Further, the influence of different design parameters on frequency, RF output power, and efficiency are analysed through Particle-In-Cell simulations.

Keywords: Overmoded; Rectangular resonant reflector; Slow-wave structure; Trapezoidal resonant reflector

1. INTRODUCTION

High power microwave (HPM) sources are extensively used for potential applications in Directed Energy Weapons (DEW), high-power radars, particle accelerators, plasma heating, etc.¹. In HPM technology, Cherenkov radiation-based RBWO is a favourable HPM source that can generate GW power levels. Non-overmoded ($D \approx \lambda$) relativistic backward wave oscillator (RBWO) is not effective at very high power levels because RF breakdown occurs as the RF electric field increases around the slow-wave structure (SWS) and inside rectangular resonant reflector (RR)²⁻³. The resulting electric field limits microwave output. The high RF output power is achieved by reducing the internal electric field, and it can also be achieved by increasing D/λ (D is SWS transverse diameter, and λ is wavelength) ratio to more than one. In addition to the overmoded SWS, a trapezoidal resonant reflector (TRR) is used to replace the RR for higher RF output power. The internal electric field can be reduced below the breakdown level by combining the two structures mentioned above²⁻³.

Swegle⁴, *et al.* and Levush⁵, *et al.* introduced a linear and non-linear analysis of RBWO. An experimentally studied a pulsed resonance RBWO for the decimeter wavelength range using a cut-off neck reflector by Kitsanov⁶, *et al.*, achieved 5 GW RF output power and 30% conversion efficiency at 3.6 GHz for a 1.2 MV DC pulse. An enhanced frequency tunability RBWO is having RR was demonstrated by Kitsanov⁷, *et al.* with 4 ± 1 GW power at 3.6 GHz and efficiency 25 % experimentally, while 32 % through Particle-In-Cell (PIC) simulation for the

beam values of 1.2 MV, 15 kA. Tot'meninov⁸, *et al.* have experimentally demonstrated the repetitively pulsed (1 s, 50 Hz) RBWO generating 2.5 ± 0.6 GW RF power with 9 % pulse-to-pulse frequency tuning centered about 3.6 GHz with 1.0 MV, 10 kA electron beam.

In this paper, an overmoded RBWO with TRR is presented in S-band to achieve high RF output power and conversion efficiency compared to RBWO with RR and cut-off neck. PIC simulation of MAGIC 3D software is used to investigate the effects of overmoded RBWO with TRR on frequency, RF output power, and efficiency. The MAGIC 3D code is based on the finite difference time domain (FDTD) method. The paper is structured in the following: Modelling and PIC simulation of overmoded RBWO with TRR is presented in Section 2, Parametric Analysis on RF output power, efficiency, and frequency with different design parameters are investigated in Section 3, and the conclusion is given in Section 4.

2. MODELLING AND PIC SIMULATION OF OVERMODED RBWO WITH TRR

The 2D configuration of overmoded RBWO with TRR is represented in Fig. 1. It is made up of a reflector, drift section, SWS, collector, and a cathode. In this section, the main components responsible for microwave generation with high efficiency are discussed, namely a) overmode SWS, b) TRR, and c) drift section. The 2D model of the structure with the electron beam given in Fig. 2 is produced using the PHASE SPACE command. The emitted electron beam from the cathode interacts with the TRR, SWS and bombards the collector's inner wall.

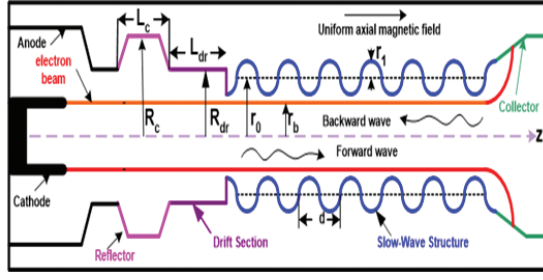


Figure 1. Schematic view of RBWO with overmoded SWS and TRR.

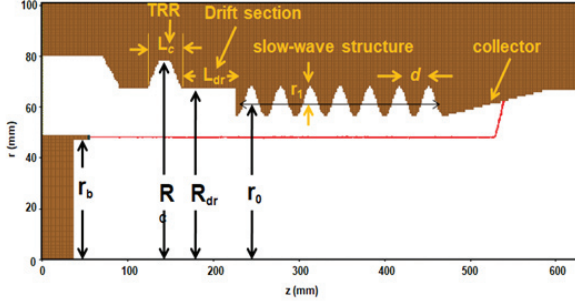


Figure 2. The simulation model of RBWO having an electron beam.

2.1 Overmoded Slow-Wave Structure (SWS)

The SWS is made up of the overmode rate ($D/\lambda \approx 1.5$). The overmoded SWS having a wall radius $r(z) = r_0 + r_1 \sin(kz)$ where $d \approx \lambda/2$ ($k = 2\pi/d$), and $2r_0 \approx 1.5\lambda$ are period and diameter of SWS, and $\lambda/16 \leq r_1 \leq \lambda/8$ is the corrugation depth. The SWS has sinusoidal corrugation with a uniform arrangement of seven periods. The sinusoidal shape is created using the FUNCTIONAL VOLUME command. The SWS provides the Cherenkov synchronisation between wave and electron by pairing down the electromagnetic wave phase velocity and beam velocity. In general, RBWO operates in the -1^{st} harmonic of the backward wave at TM_{01} mode line, and $\sim \pi$ mode is selected for obtaining higher interaction impedance⁴.

$$D_{ln} = \left(\frac{\omega^2 - k_n^2 c^2}{k_{\perp n}^2 c^2} \right) \left[I_{0ln} - \alpha \left(\frac{ck_{\perp n}}{\omega - k_n v_b} \right)^2 \times J_0(k_{\perp n} r_b) \right] \quad (1)$$

$$\left[I_{0ln} Y_0(k_{\perp n} r_b) - K_{0ln} J_0(k_{\perp n} r_b) \right]$$

The TM_{01} mode line interaction with beam mode line obtained⁴ with $\alpha = I_b = 0$ in (1) as shown in Fig. 3. where r_b is electron beam radius, l and n are model space and Floquet's spatial harmonics, v_b and c are the velocity of beam and light, α is the space-charge factor, $\omega = 2\pi f$, J_0 and Y_0 are Bessel and Neumann function of the order zero, I_{0ln} and K_{0ln} are fourier integrals of the Bessel and Neumann function, k_l and k_n are the axial wave numbers for the l^{th} and n^{th} harmonics respectively, and $k_{\perp n} = \sqrt{(\omega/c)^2 - k_n^2}$ is the transverse wave number of the n^{th} spatial harmonics. Figure 3 shows that the beam mode line ($\omega = k_z v_b$), which is intersecting nearer to π -point on the line of TM_{01} mode for the beam energy 1.2 MeV, and the corresponding frequency is ~ 3.6 GHz.

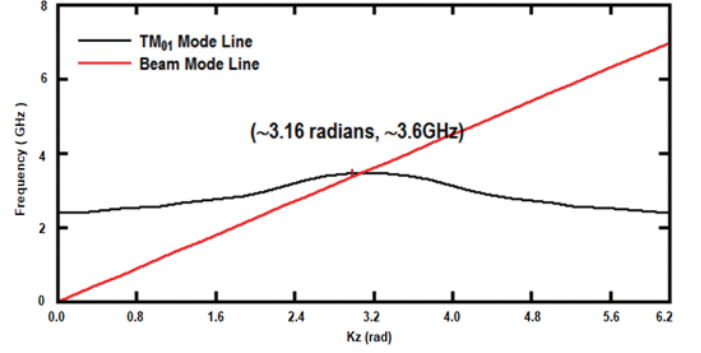


Figure 3. The dispersion curve of the beam mode line (1.2 MV) with the TM_{01} mode line (overmoded SWS).

2.2 Trapezoidal Resonant Reflector (TRR)

The reflector is used to reflect the generated TM_{01} mode by the interaction of -1^{st} harmonic of RF wave and slow space charge wave accompanied with a beam traveling towards collector (forward direction), and lock TM_{02} mode⁹. The dimensions of TRR (Fig. 2) are obtained using $R_c \leq \chi_{mn} c / 2\pi f$ (radius) and $L_c \leq \lambda/3$ (length) respectively, where, χ_{mn} is the TM_{02} mode eigenvalue, and f is the operating frequency. The TRR is designed to specify the volume generated by a stencil rotation around the symmetry axis with the VOLUME ROTATE command. With the development of TRR, the absolute electric field in the reflector region is decreased from ~ 200 kV/cm in RR (Fig.4(a)) to ~ 120 kV/cm (Fig. 4(b)). This reduces the radial momentum spread and improves the bunching by enhancing the electron beam pre-modulation, which in turn increases the RF output power^{3,10}. The radius of both TRR and RR are the same, and the length of TRR is adjusted to resonant frequency by slanting the sidewalls of the RR, as shown in Fig. 4 (b).

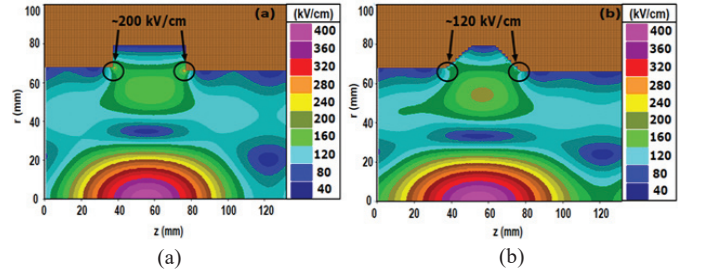


Figure 4. Absolute electric field distribution in contour of a cold test, (a) RR and (b) TRR.

2.3 Drift Section

The drift section (L_{dr}) between the SWS and TRR showed in Fig. 2 is modelled using the conformal volume command 'VOLUME'. To achieve the desired TM_{01} mode interaction and excellent beam-wave modulation, the dimensions of the radius and length of the drift section are calculated using $\chi_{01} c / 2\pi f \leq R_{dr} < \chi_{02} c / 2\pi f$ and $L_{dr} \approx \lambda$, respectively.

2.4 Simulation Results

The RBWO output RF power enhanced with TRR and overmoded SWS. The optimised parameters of Fig. 2 are shown in Table 1. The RF output power ~ 5.4 GW calculated is the average power at the end port area of the device with

Table 1. Design parameters of overmoded SWS and TRR^{6,7}

	Parameter	Symbol	Values (mm)
Overmoded SWS	Mean radius	r_0	62.50
	Corrugation amplitude	r_1	6
	Period	d	36
	SWS length	$N(7*d)$	252
Reflector	Length	L_c	40
	Radius	R_c	79.5
	Drift length	L_{dr}	63.8

OBSERVE FIELD_POWER S.DA FILTER STEP command as shown in Fig. 5 (blue color) with a conversion efficiency ~33 %. The RF output power of the overmoded RBWO with RR limited to ~5 GW is also shown in Fig. 5 (red color) with a conversion efficiency of ~32 %. The developed beam current ~13.5 kA is measured with the 1.2 MV of input DC pulse. An external magnetic field 2.0 T is applied for confining the beam. The obtained RF output power curve is smooth without any disturbance after the saturation. The frequency spectrum (Fig. 6(a)) of the corresponding radiated power is calculated by the command OBSERVE FIELD_INTEGRAL E.DL at the end of the device and applying the Fast Fourier Transform (FFT) with a frequency window 0 to 10 GHz. The frequency-time plot for the obtained RF output power is observed in Fig. 6(b). The frequency spectrum and frequency-time plots indicate no mode competition, and no harmonics are generated for the device total simulation. Figure 7 shows the generated output mode with both vector and contour plot at 55 ns, which is a pure fundamental TM_{01} mode. Other unwanted modes are eliminated by adequately designing the corrugation amplitude of the SWS².

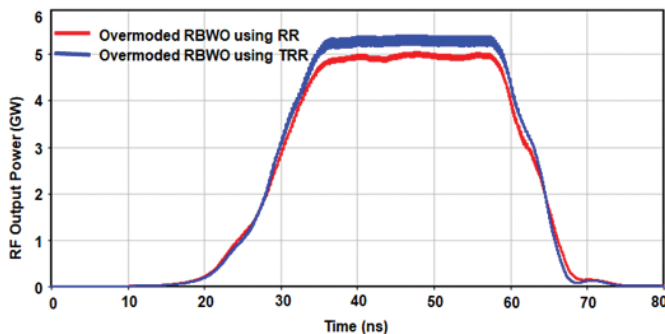


Figure 5. RF output powers for the overmoded RBWO with different reflectors.

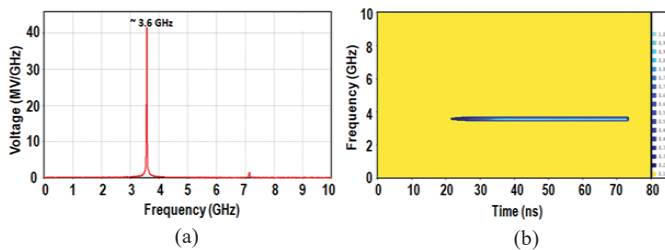


Figure 6. (a) Frequency spectrum and (b) The time-frequency of the electric field.

3. PARAMETRIC ANALYSIS

In this section, the sensitivity of the device with different design specifications consist of beam voltage, corrugation amplitude, drift length, and the magnetic field is studied.

3.1 Beam Voltage (V_b)

As the beam voltage increases, both output RF power, and efficiency increase. The increasing the beam voltage, more RF output power is generated, but the efficiency decreases shown in Fig. 8(a). The reduction in the device efficiency is that the beam mode line shifted towards the left and right from the operating $\sim \pi$ -point with the increase and decrease in voltage, respectively. The change in π -point is because of a change in beam velocity with the beam voltage ($\omega = k_z v_b$) that causes the degradation of beam-wave synchronism interaction. The direct effect of reduction in efficiency due to an increase in the developed beam current as observed in Fig. 9.

Figure 8(b) indicated the variation of the frequency w.r.t the beam voltage. The beam voltage between 0.6 MV and 2.0 MV, the operating frequency is almost constant. The operating

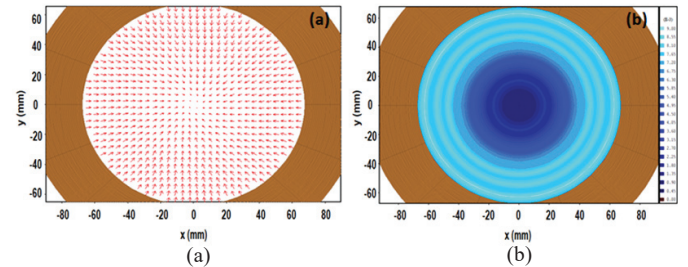


Figure 7. Fundamental TM_{01} mode electric field distribution of (a) vector and (b) contour plot.

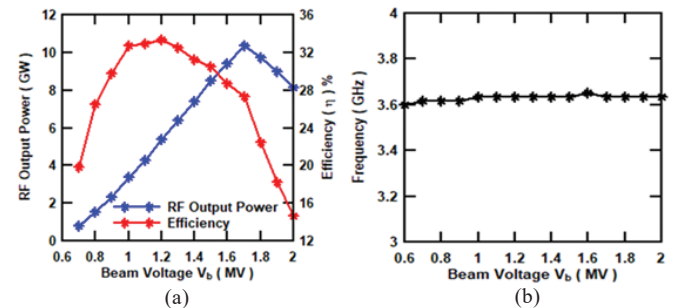


Figure 8. Beam voltage depends on (a) RF output power and efficiency and (b) frequency.

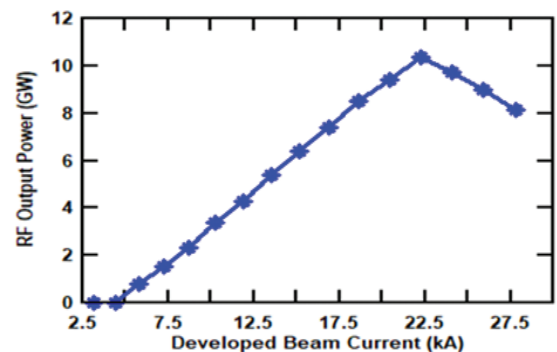


Figure 9. Influence of developed beam current on RF output power.

voltage is optimised to 1.2 MV for RF power ~ 5.4 GW and efficiency $\sim 33\%$ at ~ 3.6 GHz.

3.2 Corrugation Amplitude (r_0)

The operating TM_{01} mode frequency decreases as the corrugation amplitude increases for different SWS periods (d) varied from 35 mm to 37 mm, as shown in Fig. 10(a). The decrease in frequency improves the separation of TM_{01} from the subsequent next higher mode, *i.e.*, TM_{02} . This results in higher RF output power in the desired operating TM_{01} mode for the value of r_1 from 5 mm to 6 mm (Fig. 10(b)). Further, the increase in corrugation amplitude more than 6 mm reduces the frequency. It decreases the RF output power because in the beam-wave synchronism interruption as the generated frequency is also affected with r_1 (Fig. 10(a)). The beam-wave interaction also gets non-synchronised due to the shift in π -point, as the period of SWS is varied. The optimised RF output power (Fig. 10(b)) generated for $r_1 = 6$ mm and $d = 36$ mm.

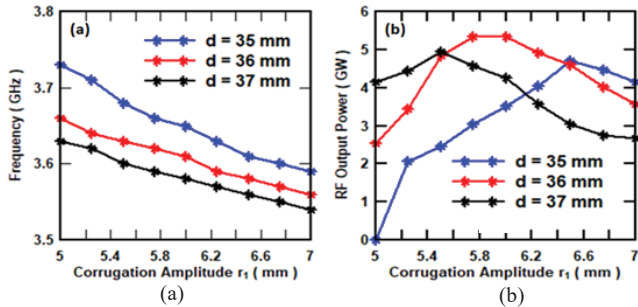


Figure 10. Influence of corrugation amplitude on (a) frequency and (b) RF output power with different periods.

3.3 Drift Length (L_{dr})

The frequency and RF output power for different drift lengths are shown in Fig. 11. The two spikes of the RF output power (blue color) were obtained due to phase synchronisation of the beam and -1^{st} space harmonic of TM_{01} mode for the various optimal drift length (L_{dr})⁶. It is observed that the maximum phase synchronisation is occurred for $L_{dr} = 63.8$ mm. The $\sim 8\%$ (Fig. 11) tuning achieved around the center frequency between 5 mm and 80 mm of the drift length.

3.4 Magnetic Field (B)

To achieve maximum RF output power, PIC simulation is used to generate the relation between RF output power and magnetic field (Fig. 12). The cyclotron synchronism occurred at B_1 and B_2 . Both are between the cyclotron mode line and forward wave fundamental space harmonics, and the cyclotron mode line and backward wave fundamental space harmonic. The cyclotron absorption of RF output power is observed at $B_1 \approx 0.12$ T and B_2 ranging 0.7 T - 0.9 T. The B_1 and B_2 values are well-matched with calculated values given by¹¹

$$B_1 = \frac{2mc\gamma_0 v_z}{ed} \left(\frac{\pi}{d} - k_z \right) \quad (2)$$

$$B_2 \approx \frac{2\pi mc\gamma_0 v_z}{ed} \quad (3)$$

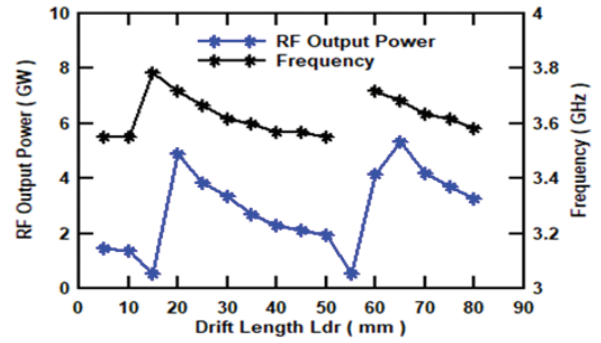


Figure 11. RF output power and frequency w.r.t drift length.

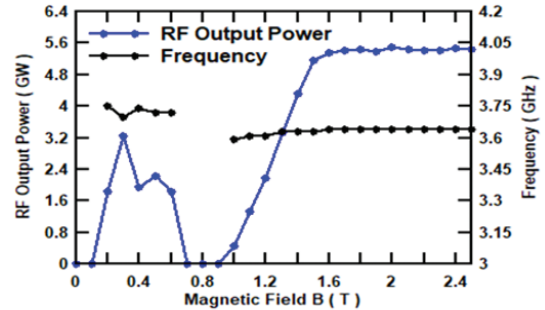


Figure 12. RF output power and frequency w.r.t magnetic field.

where k_z and v_z are fundamental spatial harmonics of longitudinal wave number and electron longitudinal velocity. The two unwanted cyclotron synchronism resulted in the suppression of output RF power observed in Fig. 12. The maximum and saturated output RF power is obtained at 2.0 T.

4. CONCLUSION

The simulation investigations of an S-band overmoded RBWO with TRR has been performed by using an FDTD based 3D electromagnetic code. TRR has reduced the absolute electric field upstream of RBWO, hence improved the power output and the conversion efficiency. In the present simulation, an efficiency of $\sim 33\%$ for output RF power of ~ 5.4 GW at ~ 3.6 GHz has been obtained. The beam voltage 1.2 MV applied, and ~ 13.50 kA beam current developed. Further, the parametric studies were performed to check the device susceptibility with the variation of beam voltage, corrugation amplitude, drift length, and magnetic field. The performance of the proposed device is compared with the earlier works as listed in Table 2.

Table 2. Comparison of proposed work with previous works

Parameters	Ref ⁶	Ref ⁷	Proposed work
Structural parameters			
Reflector	Cut-off neck	RR	TRR
Electrical parameters			
Beam voltage	1.2 MV	1.2 MV	1.2 MV
Developed beam current	~ 15 kA	~ 15 kA	~ 13.50 kA
Output parameters			
Operating frequency	3.6 GHz	3.6 GHz	~ 3.6 GHz
Output RF power	~ 5 GW	4 ± 1 GW	~ 5.4 GW
Efficiency	$\sim 30.00\%$	$\sim 32.00\%$	$\sim 33.00\%$

REFERENCES

1. Benford, J.; Swegle, J.A & Schamiloglu, E. High Power Microwaves. Taylor & Francis, New York, 2006.
doi: 10.1201/9781420012064
2. Abe, D.K; Carmel, Y.; Miller, S.M; Bromborsky, A.; Levush, B.; Antonsen, T.M & Destler, W.W. Experimental studies of overmoded relativistic backward-wave oscillators. *IEEE Trans. Plasma Sci.*, 1998, **26**(3), 591–604.
doi: 10.1109/27.700796
3. Cao, Y.; Sun, J.; Teng, Y.; Zhang, Y.; Zhang, L.; Shi, Y.; Ye, H. & Chen, C. A powerful reflector in relativistic backward wave oscillator. *Phys. Plasmas*, 2014, **21**, 093106(1)–093106(4).
doi: 10.1063/1.4895660
4. Swegle, J.A; Poukey, J.W & Leifeste, G.T. Backward-wave oscillators with rippled wall resonators: Analytic theory and numerical simulation. *Phys. Fluids*, 1985, **28**(9), 2882–2894.
doi: 10.1063/1.865209
5. Levush, B.; Antonsen, T.M; Bromborsky, A.; Lou, W.R & Carmel, Y. Theory of relativistic backward-wave oscillators with end reflections. *IEEE Trans. Plasma Sci.*, 1992, **20**(3), 263–280.
doi: 10.1109/27.142828
6. Kitsanov, S.A; Klimov, A.I; Korovin, S.D; Kurkan, I.K; Pegel', I.V & Polevin, S.D. Pulsed 5-GW resonance relativistic BWT for a decimeter wavelength range. *Tech. Phys. Lett.*, 2003, **29**(6), 87–94.
doi: 10.1134/1.1565652
7. Kitsanov, S.A; Klimov, A.I; Korovin, S.D; Rostov, V.V & Tot'meninov, E.M. Relativistic BWO with enhanced frequency tunability. *IEEE Trans. Plasma Sci.*, 2005 **33**(5), 1685–1689.
doi: 10.1109/TPS.2005.856421
8. Tot'meninov, E.M; Klimov, A.I; Kurkan, I.K; Polevin, S.D & Rostov, V.V. Repetitively pulsed relativistic BWO with enhanced mechanical frequency tunability. *IEEE Trans. Plasma Sci.*, 2008, **36** (5), 2609–2612.
doi: 10.1109/TPS.2008.2004239
9. Choyal, Y; Parmar, N.; Saini, A.K.; Chhotray, S. K; Bhat, K.S & Kumar, L. Simulation study of resonant reflector for S-band BWO. *J. Phys., Conf. Ser.*, 2012, **365**, (1), 012055.
doi: 10.1088/1742-6596/365/1/012055
10. Li, X.; Song, W.; Tan, W.; Zhang, L.; Su, J.; Zhu, X.; Hu, X.; Shen, Z.; Liang, X. & Ning, Q. Design of a high efficiency relativistic backward wave oscillator with low guiding magnetic field. *Phys. Plasmas*, 2016, **23**(7), 073101(1)–073101(6).
doi: 10.1063/1.4954903
11. Vlasov, A.N.; Ilyin, A.S & Carmel, Y. Cyclotron effects in relativistic backward-wave oscillators operating at low magnetic fields. *IEEE Trans. Plasma Sci.*, 1998, **26**(3), 605–614.
doi: 10.1109/27.700797

CONTRIBUTORS

Mr V. Venkata Reddy received his BTech from JNTU Hyderabad, India, in 2007, and the ME from Anna University, Chennai, India, in 2010. He is currently pursuing PhD in microwave engineering at IIT (BHU) Varanasi, Varanasi, India. His current research interest includes high-power microwave devices and periodic waveguide structures.

In the current study, he has designed and simulated an overmoded RBWO using TRR. He has compared RF output power of overmoded RBWO using TRR with overmoded RBWO using RR and performed a parametric simulation of RBWO using TRR.

Mr M.A. Ansari received his BTech in electronics and communication engineering from Maharshi Dayanand University, Rohtak, India, in 2014. He is currently pursuing Ph.D.degree in electronics engineering at IIT (BHU) Varanasi, Varanasi, India.

His current research interest includes high power microwave sources, periodic structures, and computational electromagnetics. In the current study, he has extended design and simulation support and revised the manuscript.

Dr M. Thottappan received his PhD in microwave engineering from the IIT (BHU) Varanasi, Varanasi, India, in 2013. He is currently an Associate Professor with the Department of Electronics Engineering, IIT(BHU) Varanasi. His current research interests include fast-wave electron beam devices, including gyrotron amplifiers and sources, high-power microwave (HPM) sources, and their subassemblies.

In the current study, he has supervised the present research work and helped in manuscript drafting.